

Design of frequency-based controllers for vibration mitigation at the Gemini-South telescope

Andres Guesalaga^{1*}, Benoit Neichel², Francois Rigaut², James Osborn¹, Dani Guzman¹

¹Universidad Católica de Chile, 4860 Vicuna Mackenna, Casilla 7820436, Santiago, Chile

²Gemini Observatory Southern Operations Center, Colina el Pino s/n, Casilla 603, La Serena, Chile

*corresponding author: aguesala@ing.puc.cl

ABSTRACT

Reduction of tip and tilt vibrations at the Gemini South MCAO System (GeMS) is addressed in this paper. A frequency framework for the synthesis of controllers is described, with particular emphasis on the search for better closed-loop performances by minimizing a H_2 norm of the tilt residuals. Previous results have shown that modeling the turbulence via identification tools using standard AR or Laplace representations can lead to non-optimal solutions, resulting in excessive rejection of certain frequencies or an unbalanced residual spectrum due to poor modeling of vibrations. In this novel approach we reconstruct the open loop slopes (pseudo-open-loop) from on-sky data and then perform a fine tuning of the controller by finding the parameters that minimize the variance of residuals during a sequence of closed-loop runs with increasing controller complexity. Although the method is not optimal, it effectively rejects the main vibrations in the loop and it also improves the overall performance of the system. The method is compared to two standard integrators: one with fixed gain and the other with optimized integral gain. Results show substantial improvements of this new method when compared to the classical integrator.

Keywords: Adaptive optics, vibration, control

1. INTRODUCTION

Adaptive Optics (AO) is a sophisticated technology that has been successfully implemented to reduce the degrading effects of the Earth's atmosphere on optical astronomical observations. Nowadays, almost all large telescopes are equipped with AO, and all the future Extremely Large Telescopes are based on this technology. As AO systems become better at correcting the atmospheric turbulence, other factors such as vibrations in the instruments and the telescope itself become increasingly important to gain the next step in performance. This is especially true for exo-planet AO systems where the residual wavefront error is very low, but it might also impact significantly the performance of other AO systems¹⁻⁵.

Vibrations can be caused by many different situations like wind shaking of the telescope structure, mechanical components in the instruments (e.g. fans, cryo-cooler and motors), or even telescope tracking errors. Identifying the source of the vibration can be difficult, and usually requires extensive measurements and specific equipment such as accelerometers or dedicated wavefront sensors (WFS). Moreover, mechanical damping is not always possible. In that case, recent studies suggest the use of control techniques to enhance AO performance in the presence of vibrations⁶. As an AO system can correct for the turbulence, the same active devices can be used to compensate for other sources of perturbations. These techniques have been successfully implemented and tested at laboratory level⁷ and have recently been introduced to operational systems^{8,9}. For the future Extremely Large Telescopes, advanced controllers are considered as the baseline for vibration rejection⁸⁻¹¹.

In this paper we describe the application of this approach on the multi-conjugate AO system (GeMS), installed at the Gemini South Observatory. We use closed-loop data obtained from on-sky runs to test control algorithms off-line and under different disturbance scenarios. Two control laws have been implemented: the classic integrator¹² and H_2 ¹³

synthesis methods. While most of the recent research effort to cope with vibrations has been concentrated in LQG control laws^{14,15} here we propose and test the H_2 synthesis methods as an alternative.

In previous work¹⁶ we have found that substantial gains in performance can be achieved with advanced controllers when they are properly designed. When large model errors are present in these techniques, the gains in performance provided by the advanced controllers are lost, showing no clear difference to the classical integrator. This emphasizes the need for on-line identification or tuning procedures that would ensure optimality in performance. We think that together with standard identification tools, the variance of the slopes residuals can be used as a minimization index to tune the controllers. This assumption is supported by two facts:

- (i) In spite of identifying the disturbance models correctly, very often the residual PSD differs from the expected flat response of LQG, H_2 or H_∞ methods. This is due not only to the varying characteristics of the disturbance, but also by unmodeled dynamics or non-linearities in the AO components.
- (ii) According to Bode's theorem and H_2/H_∞ theory, imbalances in the closed-loop residual spectrum will take the performance away from the optimum. For instance, over-rejected frequencies worsen the performance in other part of the spectrum.

This article proposes a solution to this problem using controllers synthesized with H_2 methods that use the minimization of the slopes' residual variance instead of trying to accurately identify the structure and parameters of the disturbance model, and the subsequent design of the associated controller.

The structure of the paper is as follows: in section 2 we describe the GeMS instrument. In section 3 we describe the theory behind each of the controllers implemented here. In section 4 we explain the implementation process of the controllers; section 5 presents the results from two test cases using on-sky data. Finally in section 6, conclusions are stated and some ideas for further work are given.

2. INTRODUCTION TO GEMS

GeMS is the Gemini multi-conjugate AO system. A schematic view of the main components is shown in figure 1.

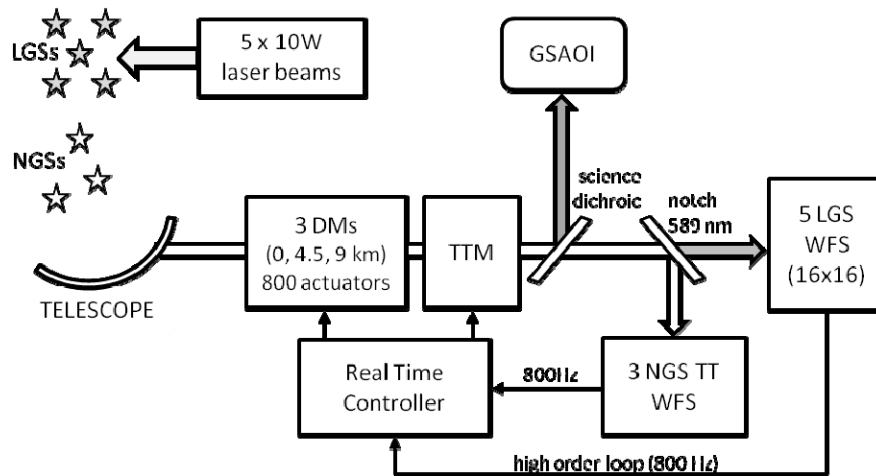


Figure 1. GeMS.

GeMS uses 5 artificial Laser Guide Stars (LGS) with their associated LGS wavefront sensors (LGSWFS) and 3 Deformable Mirrors (DM) to compensate the turbulence over a field of view of 2 arcmin. Besides this, 3 Natural Guide Stars (NGS) are required for the control of the Tip-Tilt and plate scale modes. The NGS consists of 3 probes, each containing a reflective pyramid that acts like a quad-cell feeding a set of 4 fibers and associated avalanche photodiodes.

Three NGS wavefront sensors (NGSWFS) provide six X-Y slopes necessary to generate global tip and tilt residuals that feed a Tip-Tilt Mirror (TTM) controller residing in the Real Time Controller (RTC). Plate scale modes can also be estimated from this set of slopes¹⁷ but they are not considered in this paper. The Laser loop and the NGS loop can be driven independently at a rate of up to 800Hz. GeMS delivers a uniform, diffraction-limited corrected near-infrared image to GSAOI. More details about GeMS can be found in other papers^{18,19}.

In this paper the NGSWFS, data are acquired while the LGS loop is closed in order to get smaller spots. We use either open-loop or reconstructed open-loop data based on the combination of the residuals seen by the WFS and the commands sent to the TTM. Figure 2 shows two typical examples of reconstructed open-loop power spectral density (PSD) plots measured at the NGSWFS level.

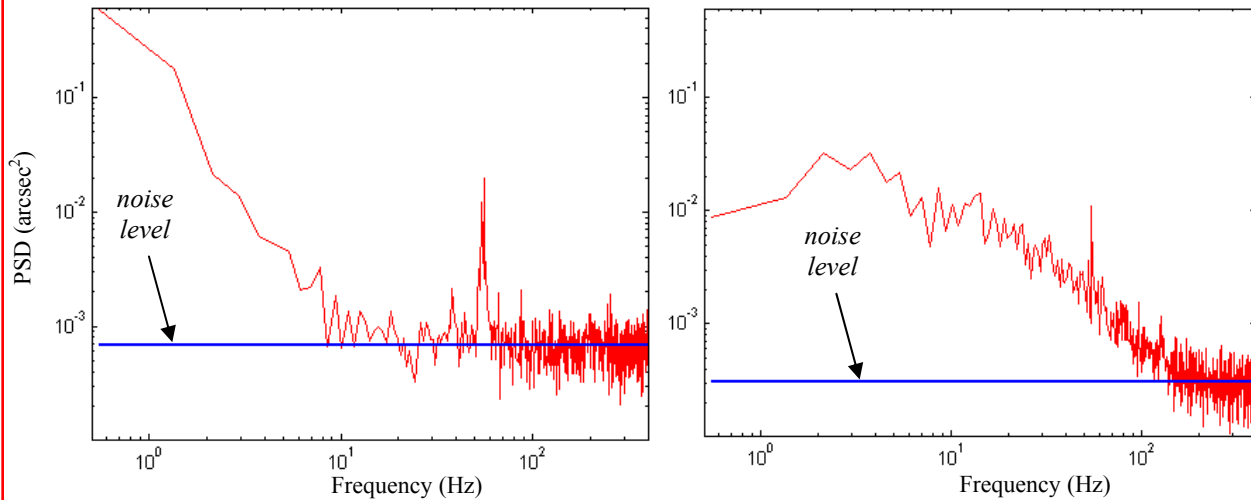


Figure 2. On-sky PSDs for the measured tilt from NGSWFS. Left: data from March 2011, Right: data acquired in April 2011. The noise level is estimated from the rms values of the residuals above 200 Hz.

These plots show a 55Hz peak in the Y-axis for on-sky data. In some examples (not illustrated here) we do also see a broad peak around 14Hz, which is believed to be induced at the top-end of the telescope, and the secondary mirror structure. This peak is not always present and may be excited by wind-shake. These two plots also illustrate the range of variation that one can expect for the turbulence's contribution. Indeed, depending on the turbulence strength and wind speed conditions, the cut-off frequency of the turbulence will vary²⁰. Notice that the turbulence energy is concentrated at lower frequencies for the slow wind case (left panel), whereas the right panel shows a displacement of the spectrum toward higher frequencies. In addition, the noise level also changes depending on the guiding star (GS) magnitudes.

In this paper we deal with tilt values only, since it is the direction where most of the disturbances occur.

3. CONTROLLER THEORY

In this section, three controllers are analyzed for a later implementation in GeMS: integrator with fixed gain; integrator with gain optimized to give the minimum residual variance, and H_2 controllers that also minimize the residual variance.

3.1. Integrator

The current default tip-tilt controller in GeMS is a classical integrator:

$$C(z) = \frac{K_i}{1 - az^{-1}}, \quad (1)$$

where z is the Z-transform operator and a is generally unity, unless a controller free from winding-up is desired (i.e. a “leaky” integrator). Parameter K_i represents the gain of the loop and is adjusted according to noise and performance requirements.

The integral controller can take two forms here: one using a fixed-gain and the other with a computed gain that minimizes the residual variance.

3.2. H_2 Control

Looking for new contributions to this challenging control problem of reducing external disturbances, we propose the use of frequency-based design techniques. These syntheses techniques based on the minimization of H_2 and H_∞ norms¹³, seem particularly suitable to tackle vibration rejection problems, since they can readily take TTM loop dynamics and performance requirements into account during the design stages.

Doyle *et al.*¹⁴ demonstrate that the computation for H_2 (reminiscent of the classical LQG problem) and the H_∞ solutions (minimization of the supreme value of a variable over the frequencies of interest) follow the same path which basically consists in solving two Ricatti equations in their static form (optimal estimation and optimal control problems). They also show that one can switch from the H_2 to the H_∞ problem by just modifying a single parameter in the algorithm.

In reference 16, we have analyzed the use of H_∞ and Kalman controllers and no significant differences have been found, save for some advantages regarding practical implementation and a better handling of high frequencies due to the easy inclusion of mirror dynamics in the problem formulation.

In this paper we have opted for the H_2 approach based on the following:

- H_2 is more intuitive, since we are minimizing a quadratic norm
- H_∞ tries to flatten the cost function (mixed norm of residuals and noise) when this may not be possible due to the mirror limited bandwidth. This can lead to solutions that departs from the optimum
- H_2 is more efficient in terms of computation, since it does not require a search for optimum as required in the H_∞ case

These last two points will be clarified in the next section.

3.2.1. The Theory

The term H_2 comes from the name of the space over which the optimization is pursued, i.e. the space of matrix-valued functions that are analytic and bounded in the open right-half of the complex plane defined by $\text{Re}(s) > 0$. Here, the control problem is presented as a mathematical optimization problem and then the H_2 synthesis technique finds it.

In the problem formulation, for a continuous-time representation, the following standard configuration is used:

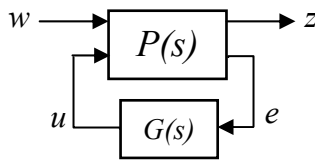


Figure 3. Standard controller-plant configuration for H_∞/H_2 synthesis.

Plant $P(s)$ has two inputs, the exogenous input w , that includes reference signal and disturbances, and the manipulated variables u . The outputs are the signals contained in vector z that we want to minimize, and the error e , that we use to control the system. The input e is used by $G(s)$ to calculate the manipulated variable u . In matrix form, the system is:

$$\begin{bmatrix} z \\ e \end{bmatrix} = P(s) \begin{bmatrix} w \\ u \end{bmatrix} = \begin{bmatrix} P_{11}(s) & P_{12}(s) \\ P_{21}(s) & P_{22}(s) \end{bmatrix} \begin{bmatrix} w \\ u \end{bmatrix}, \quad (2)$$

and

$$u = G(s) e. \quad (3)$$

The system $P(s)$ can also be represented in a compact state-space form:

$$P(s) : \begin{bmatrix} A & B_1 & B_2 \\ C_1 & D_{11} & D_{12} \\ C_2 & D_{21} & D_{22} \end{bmatrix}, \quad (4)$$

where every element in $P(s)$ is a combination of the state-space matrix and vectors, for instance, $P_{21}(s) = C_2(sI - A)^{-1}B_1 + D_{21}$. Dropping the Laplace operator s for simplicity, the output z can now be expressed in terms of the input w by:

$$z = F_l(P, G) w, \quad (5)$$

where F_l is:

$$F_l(P, G) = P_{11} + P_{12}G(I - P_{22}G)^{-1}P_{21}. \quad (6)$$

The H_2 synthesis finds a controller G such that the H_2 norm of $F_l(P, G)$ is minimized.

The H_2 -norm of $F_l(P, G)$ is defined as:

$$\|F_l(P, G)\|_2 = \left(\frac{1}{2\pi} \int_{-\infty}^{\infty} \text{trace}[F_l(P, G)(j\omega)^* \times F_l(P, G)(j\omega)] d\omega \right)^{1/2}, \quad (7)$$

The controller $G(s)$ in their state-space form, is obtained from Doyle and co-authors¹³:

$$\begin{aligned} A_K &= A - B_2 B_2' X_2 - Y_2 C_2' C_2, \\ B_K &= B_2 X_2, \\ C_K &= Y_2 C_2', \\ D_K &= 0, \end{aligned} \quad (8)$$

where X_2 and Y_2 are the solutions of two Riccati equation given by:

$$X_2 = \text{Ric} \begin{bmatrix} A & -B_2 B_2' \\ B_1 B_1' & -A \end{bmatrix}, \quad (9)$$

and

$$Y_2 = \text{Ric} \begin{bmatrix} A' & -C_2 C_2' \\ -B_1 B_1' & -A \end{bmatrix}. \quad (10)$$

3.2.2. Application of H_2 to the Tip-Tilt Problem

In this frequency approach the problem is stated as the servo-control configuration in figure 4.

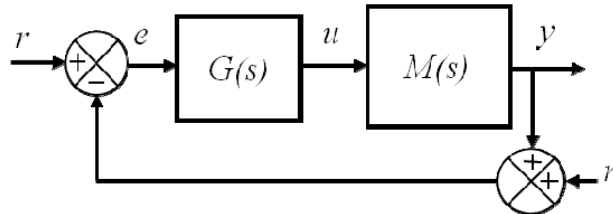


Figure 4. Servo-control problem

The setpoint r is formed by the incident tilt and disturbances (e.g. vibrations), e is the residual output of the mirror that enters controller $G(s)$ to generate the manipulated variable u to move the tip-tilt mirror whose output y is contaminated with noise n and later subtracted to the incoming r . The mirror transfer function $M(s)$ contains the dynamics of the actuator and the two-frame delay of a standard Shack-Hartmann loop.

The controller $G(s)$ is synthesized to reduce what is called the mixed-sensitivity norm. This norm is formed as a weighted combination of the Error Transfer Function or Sensitivity Function (SF), the Control Sensitivity Function (CSF) associated to control energy and the Noise Transfer Function (NTF). By defining $w = r - n$, these functions are:

$$SF(s) = \frac{e(s)}{w(s)} = \frac{1}{1 + M(s)G(s)} \quad (11)$$

$$CSF(s) = \frac{u(s)}{w(s)} = \frac{G(s)}{1 + M(s)G(s)} \quad (12)$$

$$NTF(s) = \frac{y(s)}{w(s)} = \frac{M(s)G(s)}{1 + M(s)G(s)} \quad (13)$$

In principle, the three functions can be used in the minimization process; however, we use the complementary SF and NTF functions only. The use of CSF can be also useful when special requirements or restrictions need to be imposed on the manipulated variables. We have found that in our case this is not necessary, since the bandwidth limit defined $M(s)$ already accounts for this.

The closed-loop system in figure 4 is re-arranged to form what is called the augmented representation shown in figure 5. Here, two weighting functions are added to the outputs to be minimized. Function $W_e(s)$ penalizes control errors and $W_y(s)$ weights the mirror output according to the external inputs. The latter can be used to attenuate the effect of noise amplification in the loop. These weighting functions are complementary, so that the contradictory requirements that good accuracy and noise rejection impose on the design, can be met by the resulting controller.

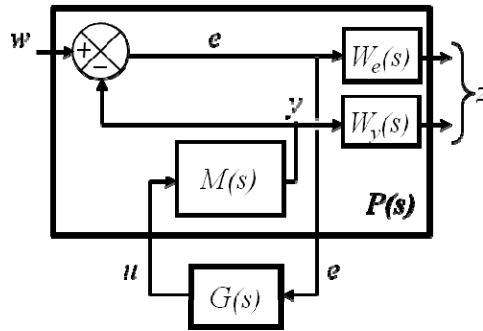


Figure 5. The augmented representation used to synthesize the H_2 controller, $G(s)$.

From the general structure in figure 4 and the arrangement of figure 5:

$$P(s) = \left[\begin{array}{c|c} P_{11}(s) & P_{12}(s) \\ \hline P_{21}(s) & P_{22}(s) \end{array} \right] = \left[\begin{array}{c|c} W_e(s) & -W_e(s)M(s) \\ \hline 0 & W_y(s)M(s) \\ \hline 1 & -M(s) \end{array} \right]. \quad (14)$$

The controller $G(s)$ is derived from the minimization of the H_2 norm in equation (7), given by:

$$\min_G \|F_l(P, G)\|_2 = \min_G \left\| \begin{matrix} W_e \cdot SF \\ W_y \cdot NSF \end{matrix} \right\|_2 \quad (15)$$

For implementation in the RTC, controller $G(s)$ is digitized using a zero-order-hold transformations.

The external disturbances are modeled with a flat spectrum and the information on the turbulence and vibration amplitude is contained in $W_e(s)$ and $W_y(s)$ so each frequency is weighted according to its intensity during the controller synthesis. This will become apparent in the next section.

4. PROCEDURE TO TUNE THE TIP-TILT LOOP

4.1. The Cost Function: Variance of Residuals

In this section we describe a sequence of steps that look for a loop tuning based on the H_2 method described above. It uses closed-loop data from on-sky observations to find a controller that minimizes the variance of the measured residuals. Since actuator values have been recorded together with the residual slopes, we can estimate the turbulence and disturbances in terms of slopes in what is known as the pseudo-open loop (POL) slopes:

$$S_k^{tur} = S_k^{res} + iMat \cdot u_{k-1} \quad , \quad (16)$$

where S_k^{tur} are the reconstructed slopes of the total turbulence and disturbances at time k , S_k^{res} are the slopes of residuals $iMat$ is the interaction matrix that models the projection of actuator commands (u_{k-1}) onto slopes of the mirror surface. Notice that the commands are delayed by one frame due to the computer processing interval and the readout of the detectors. The turbulence plots shown in figure 2 are an example of this reconstruction and they will be used to explain the tuning method.

Once the turbulence is calculated using the POL reconstruction, we can represent the turbulence and residual variables in a form compatible with input w in figure 5 using the pseudo inverse of matrix $iMat$:

$$w_k = iMat^{-1} \cdot S_k^{tur} \quad , \quad (17)$$

We can now take the Fourier transform of vector w and work in a frequency framework. Since our objective is to design a controller that minimizes the variance of the residuals, i.e.

$$\underset{G(s)}{\text{Min}} \sum_{k=0}^{N-1} |e_k|^2 \quad , \quad (18)$$

the Parseval's theorem is particularly helpful for this purpose:

$$\sum_{k=0}^{N-1} |e_k|^2 = \frac{1}{N} \sum_{k=0}^{N-1} |E(j\omega_k)|^2 \quad , \quad (19)$$

where e and E are the residuals' time and frequency vectors respectively and N is the vector length.

We now define σ_e as the variance of the residuals we want to minimize:

$$\sigma_e = \frac{1}{N} \sum_{k=0}^{N-1} |e_k|^2 \quad , \quad (20)$$

From equation (7) and Parseval's theorem, it is clear that this variable is proportional to the H_2 norm of the residuals.

Since the output weighting function W_y is independent of the controller and can be easily estimated from open-loop or POL data (amplitude at higher frequencies in figure 2), only the estimation of the weighting function W_e remains in order to find the controller. Here is where our method departs from traditional approaches^{11,21} where model-identification tools are used to represent the turbulence and vibrations, with a later controller design based on this model.

We have found that these approaches are not reliable for disturbances containing vibrations with narrow peaks. They also disregard nonlinearities or require a fixed model structure. In¹¹ an original alternative is suggested where vibrations and turbulence are treated separately. Although satisfactory results are reported, the technique requires some arbitrary definitions that limit the generalization of the method.

In other cases¹⁶, the fact of neglecting some dynamics or nonlinearities in the modeling, can yield to closed-loop behaviors that tend to over-reject certain frequencies or they do not fully eliminate them.

Our approach skips this step and looks for a controller that starting from a basic configuration (classical integrator), increases its complexity by adding filters with pre-defined structures that look for the parameters that gives the minimum residual variance in each case. This approach is not optimal but it sequentially constructs an increasingly complex controller up to a point where no further improvements in the closed-loop performance are obtained.

4.2. Loop Delay and Mirror Dynamics

The mirror transfer function, $M(s)$, contain the bandwidth of the actuators and the two-frame delay of the standard Shack-Hartmann loop. According to the manufacturer, the bandwidth of the mirror is 380 Hz. A value of 400 Hz was measured experimentally, so the dynamics of the mirror was approximated to:

$$M(s) = \frac{e^{-2\Delta s}}{0.0025s + 1}, \quad (21)$$

where Δ is the sampling interval of the sensors. In the remainder of the paper, pure delays are approximated by bilinear transformations. Dynamic modeling of the mirror is also necessary when mechanical resonances are important²².

4.3. The Tuning Sequence

The sequence of steps that form this method are described in this section. It starts with the optimization of the standard integrator, following with the synthesis of increasingly complex H_2 controllers. We use the two sets of data shown in figure 2. The results for the slow turbulence are always shown in the left panel in the following figures, whereas the ones associated to the fast turbulence are shown at the right.

4.3.1. Step 1: The Fixed Gain Integrator

This is the default controller in GeMS. The value of K_i normally ranges between 0.2 and 0.4, but it is normally fixed at $K_i = 0.2$. Parameter a is usually 1 (pure integrator).

4.3.2. Step 2: The Optimal Integrator

The search for the right tuning starts by looking for the value of K_i that gives the minimum variance of the residuals in a simulated closed-loop²³. Figure 6 plot the variance for the two types of disturbances shown in figure 2. A significant difference exists between the variance for the slow turbulence and fast turbulence.

4.3.3. Step 3: The First Order Model or Leaky Integrator

Now the controller is synthesized using the H_2 technique. By defining adequate weighting functions and the plant $M(s)$ defined in equation (21) the closed-loop is excited with the reconstructed turbulences shown in figure 2. From the sensitivity function, the residual $E(j\omega)$ can be estimated and using equations (19) and (20) a search for the controller that minimizes the variance σ_e can be implemented.

By assuming that the reconstructed slopes at higher frequencies (figure 2) are purely noise, function W_y is estimated from the average rms value of the residuals above 200 Hz. W_y is then a constant value, giving 0.026 and 0.017 arcsecs for the two turbulences in figure 2.

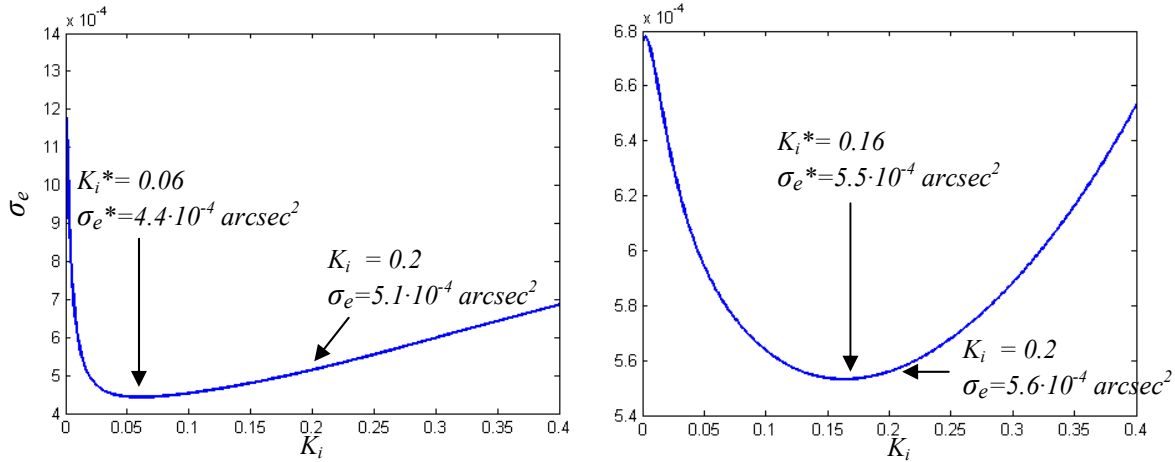


Figure 6. Step 2: Minimum σ_e for optimal integrator gain (Left: slow turbulence; Right: fast turbulence)

We then assume that the turbulence can be described by the simplest first order function:

$$W_{e3}(s) = \frac{C_0}{s + C_1}, \quad (22)$$

A search for C_0 and C_1 that minimize σ_e is carried out giving the plots in figure 7 for the two turbulence cases. The power spectrum of $E(j\omega)$ differs to that of the integral controller with fixed gain for both types of turbulence; however it is similar to the optimized integrator in the case of the slow turbulence (left panel). This is not surprising since the first order function that minimizes the residuals have very small leaky action, i.e. a very small C_1 . This is confirmed in figure 8, where the left panel shows the W_{e3} function that result from the optimal C_0 and C_1 which resembles a pure integrator (cutoff frequency lower than the visual range). On the contrary, in the right panel (fast turbulence), the fitted W_{e3} has a cutoff frequency around 10 Hz which is significantly different from the constant negative slope expected for an integral controller. It is interesting to see the effect of the different controllers in terms of the sensitivity function (SF). For the slow turbulence, the H_2 controller and the optimum controller behave almost identically, which is again due to the similarity between the W_{e3} and the frequency response of a pure integrator. However, an integral controller with a gain of $K_i = 0.2$ gives a higher bandwidth for the rejection function but a poor performance in terms of residuals (the variance for the H_2 , optimal integrator and default integrator are 0.000514, 0.000443 and 0.000442 arcsecs² respectively).

In the case of the fast turbulence, the SF of the H_2 controller departs significantly from those of the two integrators with a significant reduction of the residuals for the advanced controller (the variance of the H_2 , optimal integrator and default integrator are 0.000556, 0.000553 and 0.000429 arcsecs² in this case).

From figure 7 it is clear that there is still room for improving the residual response in order to get a more even or flat curve. For both types of turbulences, there is a strong peak due to the 55 Hz vibration and also some high residual values at lower frequencies that are tackled using H_2 synthesis in the following steps.

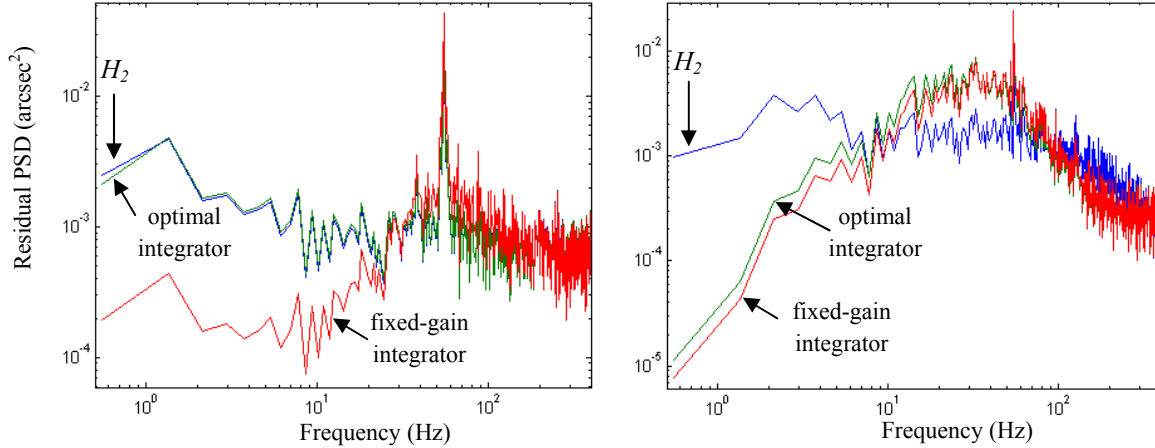


Figure 7. Step 3: residual PSD for optimum first order turbulence model. PSDs of integrator residuals are also shown

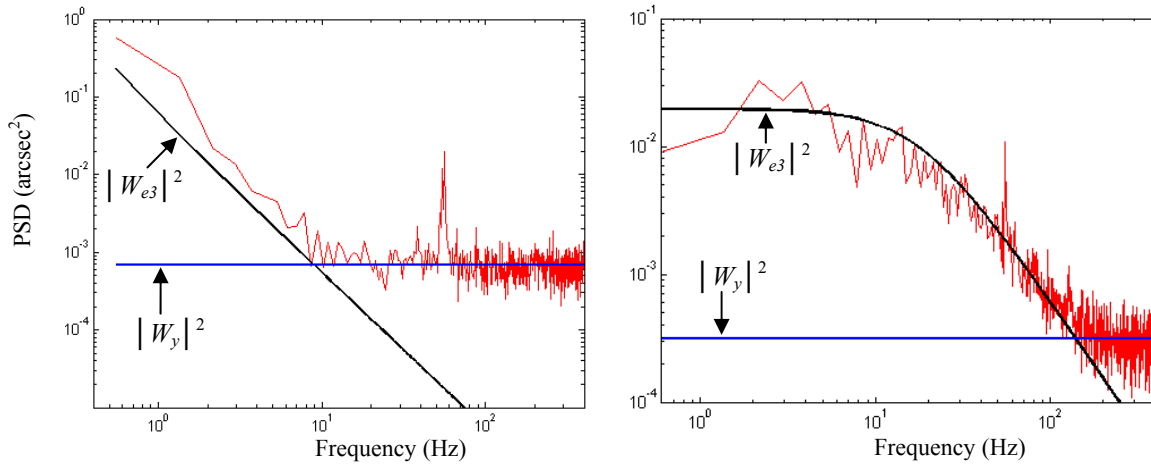


Figure 8. Step 3: Weighting functions W_{e3} and W_y that result from the optimal C_0 and C_1 values

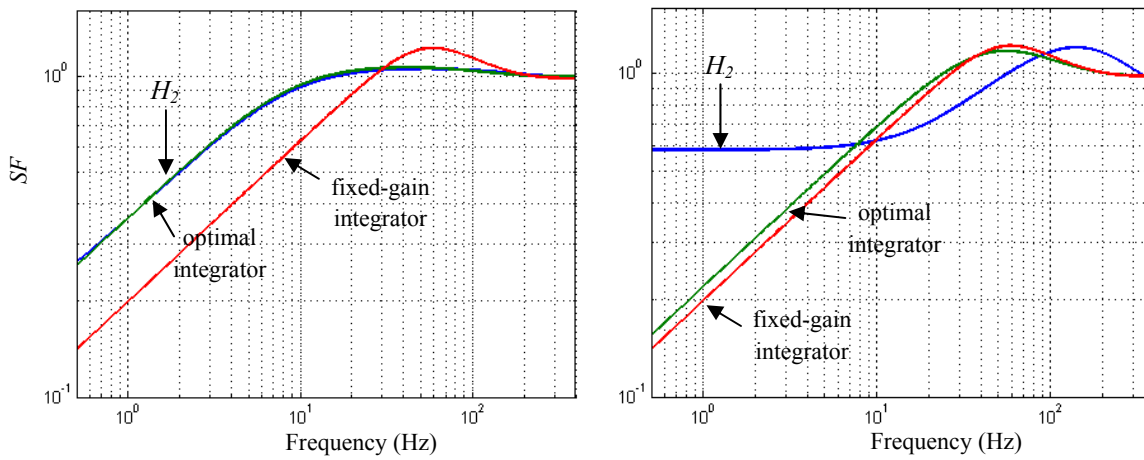


Figure 9. Step 3: Sensitivity functions for integral and H_2 controllers

4.3.4. Step 4: First Order Plus 1 Notch

A notch filter is used in the following steps to model the vibrations:

$$F_4(s) = \frac{s^2 + 2\eta_1\omega_o s + \omega_o^2}{s^2 + 2\eta_2\omega_o s + \omega_o^2}, \quad (23)$$

Examples of this function are presented in figure 10 for a vibration of $\omega_o=2\pi\cdot 50$ rad/s and for different values of η_1 and η_2 . This notch filter allows modeling a vibration in terms of amplitude and width. The left panel shows three responses for different ratios of η_1/η_2 , and in the right panel, the ratio η_1/η_2 is kept constant at 100, but three different pairs of values of η_1 and η_2 are tested.

The new function for weighting the error in the synthesis method becomes:

$$W_{e4}(s) = \frac{C_0}{s + C_1} \cdot F_4(s), \quad (24)$$

and a search for new C_0 and C_1 , together with the values of ω_o , η_1 and η_2 is implemented.

The critical part in searching for the optimal parameters is finding the vibration frequencies. Using classical identification schemes we have found that local minima tend to appear in the searching process, missing the vibration components. In¹¹, an original approach to avoid this omission is used, where a clipping technique separates vibrations from turbulence or noise. Here, we propose a scanning method that despite an increase in processing demand and lack of optimality is robust and ensures the detection of the vibrations of interest.

The method consists in scanning the spectrum within the range where vibrations are likely to exist, i.e. sweeping the complete spectrum with frequency ω_o in equation (23), for several values of η_1 and η_2 . This process is shown in figure 11, where function $F_4(s)$ (top panels) is swept from left to right, generating the corresponding variance plot (bottom panels). For each scanning value of ω_o a controller is synthesized and the subsequent closed-loop residual variance is computed. The frequency value that generates the minimum variance during this scanning process is selected for the notch rejection frequency and a search for the values of C_0 , C_1 , η_1 and η_2 that minimize the variance are sought. Notice that for both turbulences the scanning process detects the vibration frequency very clearly, generating a distinctive minimum in the variance plot, which is significantly lower than the variance obtained in step 3 (figure 11, horizontal line, bottom panels).

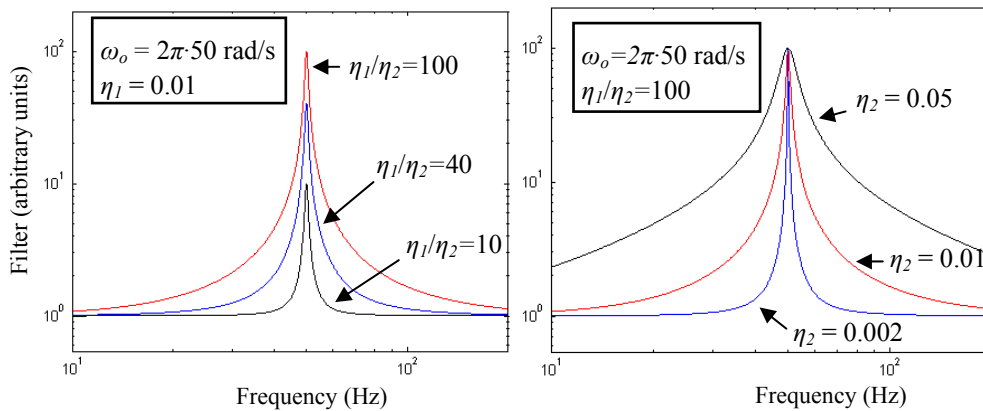


Figure 10. Frequency response of notch filters for $\omega_o=2\pi\cdot 50$ rad/s and for different values of η_1 and η_2

If the ratio η_1/η_2 is kept constant through the scanning, the noise would cover the filter peak at? higher frequencies. To avoid this, the ratio must be modified to keep a peak of constant amplitude above the sum of W_{e4} and W_y PSDs, so a “tip of the iceberg” effect is obtained in the vibration modeling (see green line in figure 12). The ratio η_1/η_2 is then:

$$\frac{\eta_1}{\eta_2} = A \sqrt{1 + \frac{W_y^2}{W_{e4}^2}}, \quad (25)$$

where A is the η_1/η_2 ratio for $W_{e4} \gg W_y$.

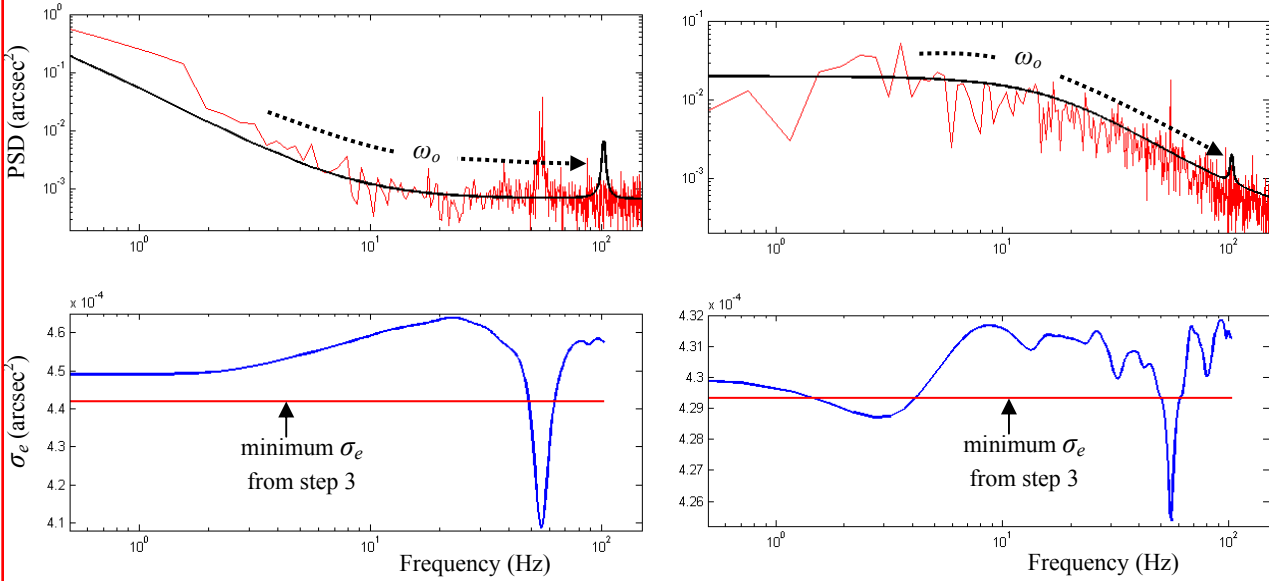


Figure 11. Step 4: scanning F_4 in search for vibrations

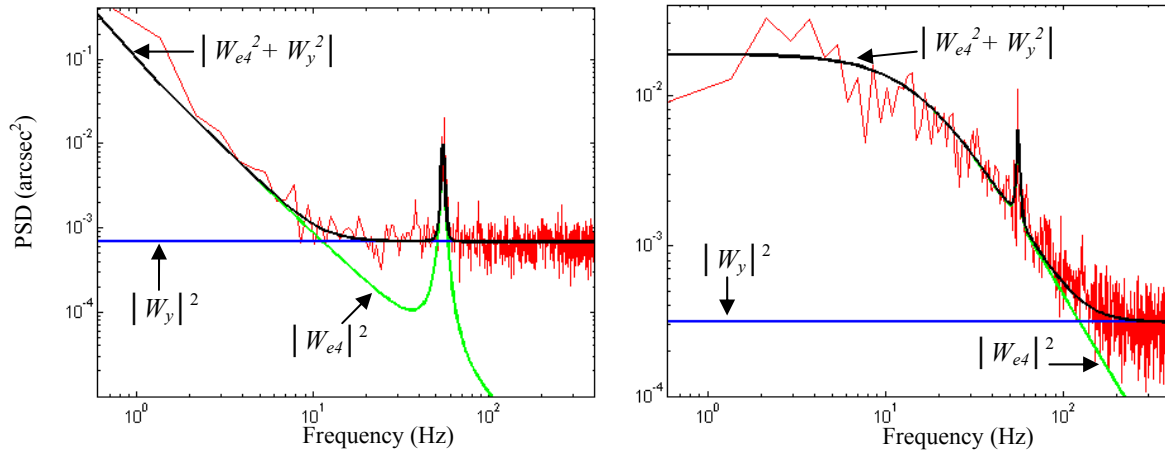


Figure 12. Step 4: PSDs of disturbances and noise for minimum variance

4.3.5. Step 5: First Order Plus 2 Notches

The following steps in the method consist in repeatedly adding complexity to the error weighting function by including additional notch filters in series, i.e. for step 5:

$$W_{e5}(s) = \frac{C_0}{s + C_1} \cdot F_4(s) \cdot F_5(s), \quad (26)$$

A new scanning process is executed, keeping the previous parameters fixed and varying the values of ω_o , η_1 and η_2 contained in $F_5(s)$ only. The result is shown in figure 13, where the minimum is achieved at lower frequencies in this case, and corresponds to a turbulence characteristic rather than a vibration. Once the value of ω_o in $F_5(s)$ has reached the minimum variance, a full search for the eight parameters in W_{e5} that give the minimum variance is performed.

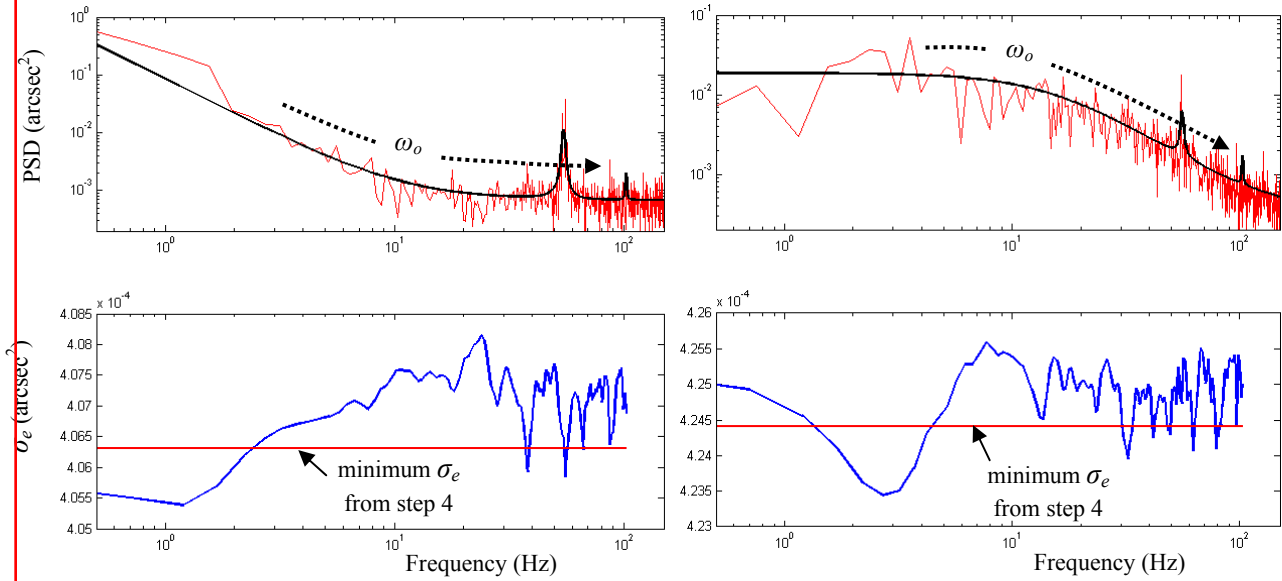


Figure 13. Step 5: scanning F_5 in search for further vibrations

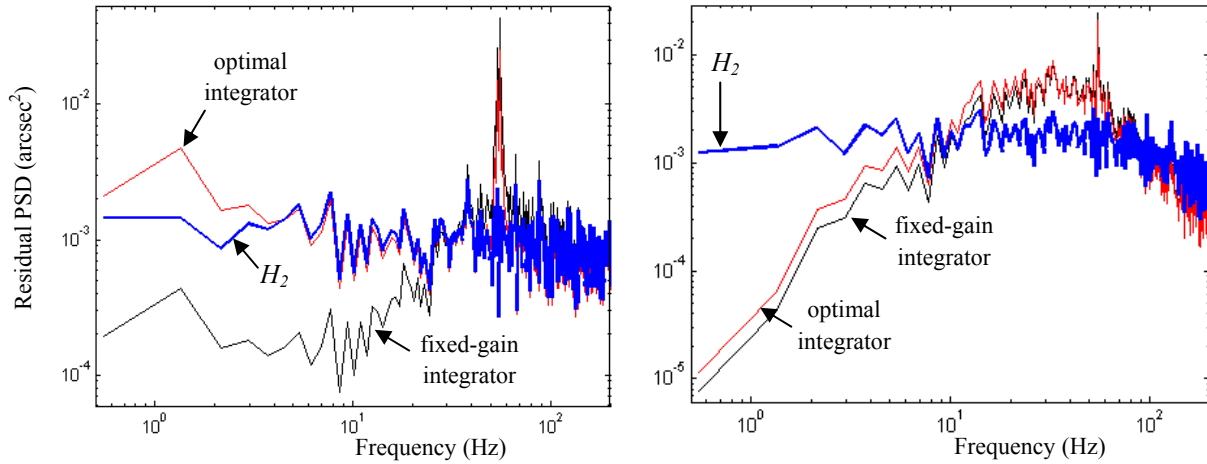


Figure 14. Step 5: residual PSD for the optimal fifth order turbulence model (F_5). Residuals' PSDs of integrators are also shown

Figure 14 shows the residual for the turbulences. Notice that not only the vibration has been fully eliminated, but also a flat response is obtained for the residual PSD, remarkably different from the integrators. Figure 14 shows a decline in the PSD of the residuals above a certain frequency, especially in the fast turbulence case (right panel). This is caused by the mirror bandwidth, which restricts the frequencies that can be effectively reduced.

An appealing feature of this method is its ability to generate good disturbances and noise models as a byproduct. Figure 15 shows the noise function W_y and disturbance W_{e5} that results from the minimization of the variance, where a very good fitting of the disturbances can be observed.

It is also interesting to see that the resulting error transfer functions (SF) in figure 16, are substantially different to the classical integrators. This is a clear example of how Bode's theorem shapes the SF to achieve a balanced frequency response. These plots also contradict the common belief that higher loop bandwidths can deliver better performances. Although this is true for the high speed turbulence (right panel), it is not for the slow turbulence (left panel).

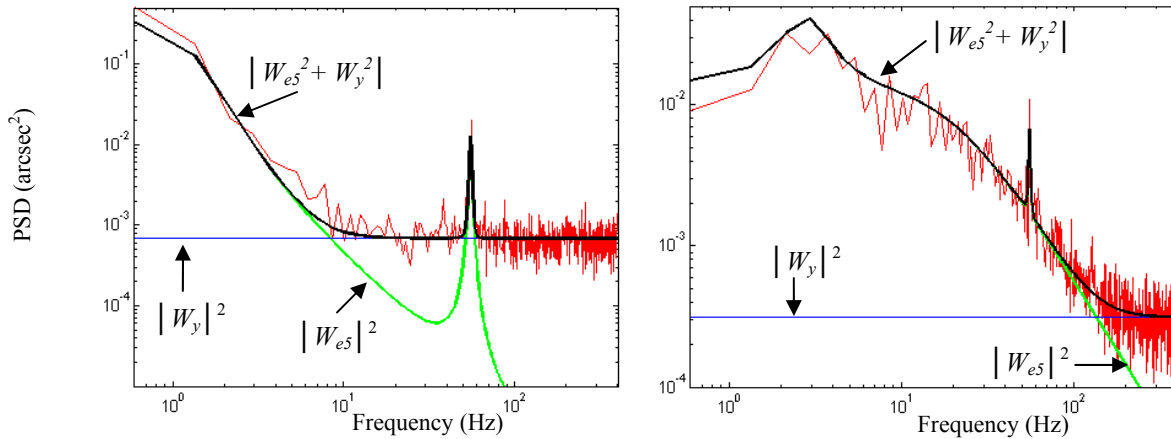


Figure 15. Step 5: PSD of disturbances and noise for the minimum variance

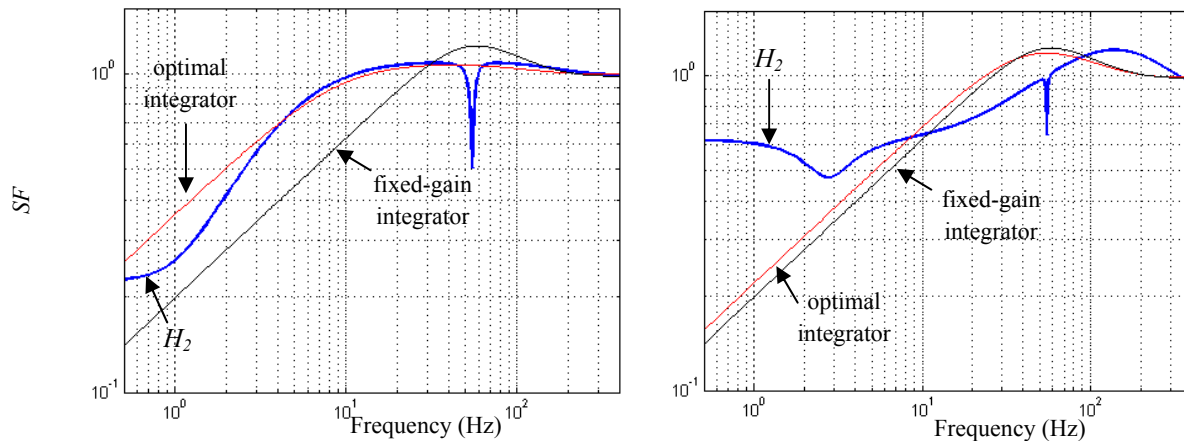


Figure 16. Step 5: Sensitivity functions for integral and final H_2 controllers

More filters can be added in series to the W_e function as long as further reductions in variance are achieved. We have found that for the turbulences analyzed here, the fifth order system defined in equation W_{e5} is sufficient. Although further improvements can be archived for higher order functions, the gain does not necessarily compensate the higher controller complexity and the longer time required to obtain a solution. This “diminishing returns” can be observed in fig. 17.

From the implementation point of view the time required to execute a complete sequence is less than 3 minutes using a commercial PC. This processing time, although adequate for the dynamics of turbulence, would represent an excessive burden for the real time controller, so a stand-alone computer would be preferable in case of a practical implementation.

We think that the extension of this technique to the control of deformable mirrors using LGSWFS information is realizable in a reasonable time scale, since the multiple loops in this case, would share many common characteristics (turbulence, vibrations, etc.), so a small number of controllers could be applied to the large number of actuator loops.

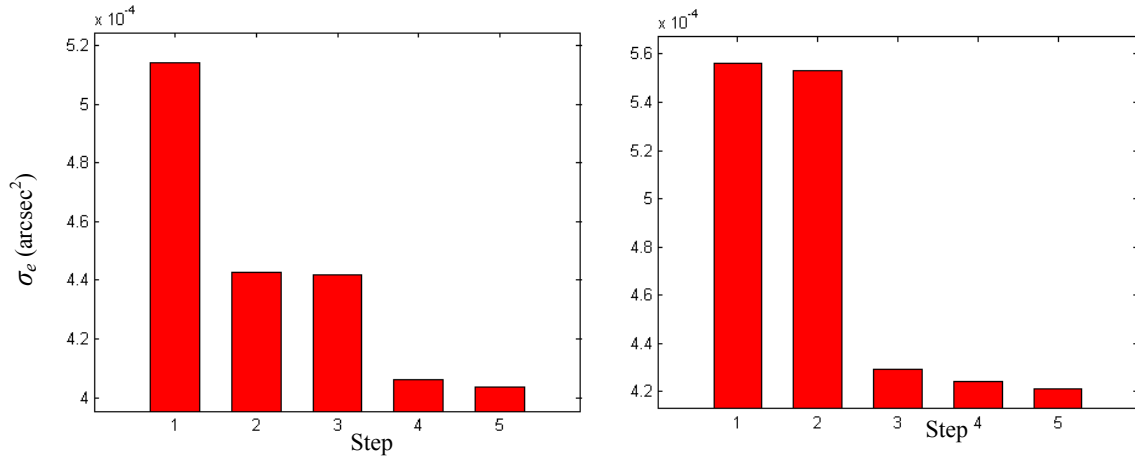


Figure 17. Progressive reduction of σ_e for the sequence of design steps

Some issues regarding a correct implementation of the method must be addressed. First, since the technique is based on the reconstruction of POL, a good knowledge of the interaction matrix $iMat$ is essential and some continuous calibration method should be developed in future work.

5. CONCLUSIONS

The principal benefit in the use of sophisticated controllers is that their SF is shaped to tackle specific frequencies where disturbances are concentrated. A balanced or nearly flat spectrum of residuals is expected in this optimal case and although the theory behind H_2 controllers ensures this, the actual results tend to miss expectations. This is mainly due to inaccurate modeling of disturbances, non-linearities or dynamics present in the loop and not modeled (e.g. mirror dynamics). This suggests that the approach of relying on accurate identification tools for finding the turbulence and vibration parameters to tune the controllers might not be the right choice, so our approach tunes the controller looking for the lowest and balanced PSD of the measured residuals on a regular basis. We have shown that there is an alternative to the identification approach which consists in synthesizing controllers that minimize the variance of residuals. By eliminating the intermediate process of model identification, our approach is free from identification errors, so a more balanced spectrum of residuals with lower variances is obtained.

Although the search for the controller that minimizes the variance of residuals has proved to be effective (flattening the spectrum measured at the NGSWFS level), our final goal is to use the spectrum measured on the science instrument itself. The next step in this line of research is to implement such tuning approach using tip-tilt information provided by the on-detector guide windows (ODGW) available in the GSAOI instrument²⁵.

ACKNOWLEDGMENTS

This work was supported by the Chilean Research Council (CONICYT) grants Fondecyt 1120626 and Anillo ACT-86.

REFERENCES

- [1] Y. Clenet, M. Kasper, N. Ageorges, C. Lidman, T. Fusco, O. P. Marco, M. Hartung, D. Mouillet, B. Koehler, G. Rousset, and N. Hubin, NAOS performances: impact of the telescope vibrations and possible origins, *Semaine de l'Astrophysique Francaise*, Paris, June 14-18, 2004.
- [2] J. Maly, E. Darren and T. Pargett, Vibration Suppression for the Gemini Planet Image, *Proceedings of the SPIE*, vol. 7733, 7731F (2010).
- [3] Y. Clenet, M.Kasper, N.Ageorges, C.Lidman, T.Fusco, G. Rousset, O.Marco, M. Hartung, D. Mouillet, B. Koehler, and N. Hubin, NACO performance: Status after 2 years of operation, *Proceedings of the SPIE*, vol. 5490 (2004).

- [4] J. P. Verán and L. Poyneer L., Evaluation of the T/T Conditions at Gemini South Using NICI AO Telemetry Data, 1st AO4ELT Conference, Paris, June 22-26, 2009.
- [5] J.Christou, C.Trujillo, B.Neichel, F.Rigaut, B.Walls, D.Coulson, J. White, A. Stephens, M. Sheehan The Effect of the Instrument Environment on the Altair AO system, 2nd AO4ELT Conference, Victoria, Canada, 25-30 Sept., 2011.
- [6] C. Petit, J.-M. Conan, C. Kulcsár, and H.F. Raynaud, Linear quadratic Gaussian control for adaptive optics and multiconjugate adaptive optics: experimental and numerical analysis, *J. Opt. Soc. Am. A* 26, 1307–1325 (2009).
- [7] C.Petit, J. M. Conan, T.Fusco, J.Montri, C.Kulcsár, H.F.Raynaud and D.Rabaud, First laboratory demonstration of closed-loop Kalman based optimal control for vibration filtering and simplified MCAO, *Proc. SPIE* vol. 6272 (2006).
- [8] B.Neichel, F.Rigaut, A.Guesalaga, I.Rodriguez, and D.Guzman, Kalman and H-infinity controllers for GeMS, Conference of the Optical Society of America on Adaptive Optics, Toronto, Canada, 10-14 July 2011.
- [9] G. Agapito, F. Quirós-Pacheco, P. Tesi, A. Riccardi, and S. Esposito, Observer-Based Control Techniques for the LBT Adaptive Optics under Telescope Vibrations, *European Journal of Control*, vol 17(3), pp. 316 – 326 (2011).
- [10] J. M. Conan, H. F. Raynaud, C. Kulcsár, S.Meimon, Are integral controllers adapted to the new era of ELT adaptive optics?, 2nd AO4ELT Conference, Victoria, Canada, 25-30 Sept., 2011.
- [11] E. Fedrigo, R. Muradore and D. Zilio, High performance adaptive optics system with fine tip/tilt control, *Control Engineering Practice*, vol. 17, pp. 122-135 (2009).
- [12] Hardy J.W., *Adaptive Optics for Astronomical Telescopes*, Oxford University Press, New York, 1998.
- [13] J. C. Doyle, K. Glover, P.P. Khargonekar, and B. A. Francis, State-space solutions to standard H₂ and H_∞ control problems, *IEEE Transactions on Automatic Control* vol. 34, pp.831-847 (1989).
- [14] B. Le Roux, J. M. Conan, C. Kulcsár, H. F. Raynaud, L. M. Mugnier and T. Fusco, Optimal Control Law for Classical and Multiconjugate Adaptive Optics, *J. Opt. Soc. Am. A*, vol. 21, no. 7, pp. 1261-1276 (2004).
- [15] C. Kulcsár, H.-F. Raynaud, C. Petit, J.-M. Conan, et P. Viaris de Lesegno. Optimal control, observers and integrators in adaptive optics. *Opt. Express*, 14(17):pp.7464-7476, 2006.
- [16] I. Rodriguez, B. Neichel, M. Hartung, T. Haywards, J. Christou, F. Rigaut, D. Guzman, A. Guesalaga, Vibration characterization and mitigation at the Gemini-South telescope, AO4ELT2 Conference, Victoria, September 2011.
- [17] B. L. Ellerbroek and F. Rigaut,, Methods for correcting tilt anisoplanatism in laser-guide-star-based multiconjugate adaptive optics, *J. Opt. Soc. Am. A*, 18, 2539-2547 (2001).
- [18] B. Neichel, F. Rigaut, M. Bec, M. Boccas, F. Daruich, C. D'Orgeville, V. Fesquet, R. Galvez, A. Garcia-Rissmann, G. Gausachs, M. Lombini, G. Perez, G. Trancho, V. Upadhyya and T. Vucina, The Gemini MCAO Systems GeMS: Nearing the End of a Lab-Story, *Proceedings SPIE* vol. 7736, no. 773606 (2010).
- [19] F. Rigaut,, Neichel B., Gemini South MCAO on-sky results, 2nd AO4ELT Conference, Victoria, Canada, 25-30 Sept., 2011.
- [20] J. M. Conan, G. Rousset and P. Y. Madec, Wave-front temporal spectra in high-resolution imaging through turbulence, *J. Opt. Soc. Am. A*, 12, 1559-1570 (1995).
- [21] S. Meimon, C. Petit, T. Fusco, and C. Kulcsár, Tip-tilt disturbance model identification for Kalman-based control scheme: application to XAO and ELT systems, *J. Opt. Soc. Am. A* , vol 27(11), pp. 122-132 (2010).
- [22] C. Correia, H. F. Raynaud, C. Kulcsár and J. M. Conan, On the optimal reconstruction and control of adaptive optical systems with mirror dynamics, *J. Opt. Soc. Am. A* , Vol. 27(2), pp. 333-349 (2010).
- [23] E. Gendron and P. Lena, Astronomical adaptive optics I. modal control optimization, *Astron. Astrophys.* 291, pp337 (1994).
- [24] B. Neichel, A. Parisot, C. Petit, T. Fusco, F. Rigaut, Identification and calibration of the interaction matrix parameters for AO and MCAO systems. This Conference [8447-209].
- [25] P. J. Young, P. McGregor, J. v. Harmelen, Using ODGWs with GSAOI: software and firmware implementation challenges. This Conference [8451-77].